An *Arabidopsis* Class II Formin, AtFH19, Nucleates Actin Assembly, Binds to the Barbed End of Actin Filaments, and Antagonizes the Effect of AtFH1 on Actin Dynamics[F]

Yiyan Zheng[1,2], Haibo Xin[3], Jinxing Lin[1], Chun-Ming Liu[1] and Shanjin Huang[1*]

[1]Key Laboratory of Plant Molecular Physiology, Institute of Botany, the Chinese Academy of Sciences, Beijing 100093, China

[2]University of Chinese Academy of Sciences, Beijing 10049, China

[3]Ornamental Horticulture and Landscape Architecture, China Agricultural University, Beijing 100094, China

[*] Corresponding Author

Tel: +86 10 62846675; Fax: +86 10 62846675; E-mail: sjhuang@ibcas.ac.cn

[F] Articles can be viewed online without a subscription.

Abstract

Formin is a major protein responsible for regulating the nucleation of actin filaments, and as such, it permits the cell to control where and when to assemble actin arrays. It is encoded by a multigene family comprising 21 members in *Arabidopsis thaliana*. The *Arabidopsis* formins can be separated into two phylogenetically-distinct classes: there are 11 class I formins and 10 class II formins. Significant questions remain unanswered regarding the molecular mechanism of actin nucleation and elongation stimulated by each formin isovariant, and how the different isovariants coordinate to regulate actin dynamics in cells. Here, we characterize a class II formin, AtFH19, biochemically. We found that AtFH19 retains all general properties of the formin family, including nucleation and barbed end capping activity. It can also generate actin filaments from a pool of actin monomers bound to profilin. However, both the nucleation and barbed end capping activities of AtFH19 are less efficient compared to those of another well-characterized formin, AtFH1. Interestingly, AtFH19 FH1FH2 competes with AtFH1 FH1FH2 in binding actin filament barbed ends, and inhibits the effect of AtFH1 FH1FH2 on actin. We thus propose a mechanism in which two quantitatively different formins coordinate to regulate actin dynamics by competing for actin filament barbed ends.

Introduction

The actin cytoskeleton has been implicated in many fundamental physiological processes including cell locomotion, cell division, cytokinesis, organelle movement, vesicle trafficking, and cytoplasmic streaming (Pollard and Borisy 2003; Pollard and Cooper 2009). These functions are intimately related to the spatial distribution and organization of the actin cytoskeleton, and require exquisite control over filament dynamics. How

actin dynamics and organization are regulated spatially and temporally is a central question in cell biology. Within cells, actin dynamics and organization are controlled by numerous actin-binding proteins (ABPs) (Pollard and Cooper 2009). Among these, actin nucleation factors allow cells to control when and where to assemble actin. Several actin nucleation factors have been identified in the published work (Carlier 2011; Firat-Karalar and Welch 2011), and the Arp2/3 complex and formin are arguably the best characterized. The Arp2/3 complex is

responsible for the formation of branched filament networks (Mullins et al. 1998), whereas formins have been shown to nucleate actin assembly for construction of parallel actin cables (Pruyne et al. 2002; Sagot et al. 2002a).

Since the initial identification of the mouse formin *limb deformity* (Kleinebrecht et al. 1982), formins have been identified from a wide variety of organisms, including plants. Formins are characterized by the presence of two conserved domains, the formin-homology domain 1 (FH1) and the FH2 domain (Higgs 2005; Higgs and Peterson 2005; Chesarone et al. 2010). The FH2 domain contains the actin-binding site, and FH1 binds to profilin and profilin-actin complexes (Pruyne et al. 2002; Sagot et al. 2002b; Li and Higgs 2003; Paul and Pollard 2008). The general activities of formins include nucleating actin filaments, binding to the barbed end of actin filaments, and facilitating actin monomer addition at the barbed end while remaining bound to the same end (Pruyne et al. 2002; Sagot et al. 2002b; Kovar et al. 2003; Zigmond et al. 2003; Higashida et al. 2004; Kovar and Pollard 2004; Romero et al. 2004; Kovar et al. 2006). The latter feature led to the establishment of a model in which formin functions as a processive actin polymerization promoting factor (Zigmond et al. 2003; Kovar and Pollard 2004; Kovar et al. 2006). However, previous studies have shown that the quantitative effects of formins on actin can vary greatly (Pruyne et al. 2002; Li and Higgs 2003; Zigmond et al. 2003; Harris et al. 2004; Romero et al. 2004; Kovar et al. 2006). In addition, novel activities have been reported for some formins. For instance, AtFH1 has been shown to be non-processive, and binds to the side of actin filaments and bundles (Michelot et al. 2005; Michelot et al. 2006). The mouse formin FRLα bundles and severs actin filaments (Harris et al. 2004; Harris et al. 2006).

Loss-of-function mutations in the Arp2/3 complex and the regulatory SCAR/WAVE complex were reported to produce phenotypes only in specific cell types, such as trichomes and epidermal pavement cells (Le et al. 2003; Li et al. 2003; Basu et al. 2005). Therefore, it is reasonable to speculate that actin nucleation and polymerization are predominantly controlled by formins in plants (Wasteneys and Yang 2004; Blanchoin and Staiger 2010). This idea is consistent with the presence of a large pool of profilin-bound actin monomers in plants, and the observation that formins are rather efficient nucleators of profilin–actin (Blanchoin and Staiger 2010). Indeed, a loss-of-function mutation in AtFH5 leads to the delay of new cell wall synthesis in endosperm (Ingouff et al. 2005), and AtFH3 controls the generation of actin cables and polarized pollen tube growth (Ye et al. 2009). Moss (*Physcomitrella patens*) For2 controls actin organization and polarized cell elongation (Vidali et al. 2009), and rice (*Oryza sativa*) FH5 regulates cell elongation and plant morphogenesis (Yang et al. 2011; Zhang et al. 2011). Collectively, these reports indicate that formins are major regulators of actin dynamics.

There are 21 formin isovariants encoded in the *Arabidopsis* genome, and they are separated into two phylogenetically-distinct classes (Cvrckova 2000; Deeks et al. 2002; Cvrckova et al. 2004; Blanchoin and Staiger 2010). Class I formins are comprised of 11 members, and are characterized by the presence of a predicted transmembrane domain at their N-termini, and class II formins are comprised of 10 members. However, the cellular and biochemical functions of most formins remain unknown. In addition, how different formin isovariants cooperate to regulate actin dynamics remains a mystery. The expected complexity of formin activities makes sequence-based predictions of the mechanism of any specific formin and the coordination of multiple formin isovariants impractical. Therefore, a direct analysis of the biochemical properties of each formin isovariant and an assessment of the coordination between different formin isovariants are urgently needed before we assume their *in vivo* functions.

Here, we cloned one member of the class II formins, AtFH19, and demonstrated that it retains the general activities of formins. However, the effect of AtFH19 on actin nucleation and elongation is less efficient compared to another well-characterized formin isovariant, AtFH1. Surprisingly, AtFH19 has an antagonizing rather than a synergistic effect on actin polymerization in the presence of AtFH1. We therefore propose a mechanism by which *Arabidopsis* formins regulate their effect on actin through the competition of different isovariants in binding to actin filaments and conferring different dynamic properties to those filaments.

Results

Generation of AtFH19 fusion proteins

Arabidopsis thaliana FORMIN19 or AtFH19 (TAIR accession no. At5g07780) is a member of the class α formins (Cvrckova et al. 2004; Grunt et al. 2008). It is comprised of a typical FH1 domain (amino acids (a.a.) 14–67) implicated in binding to profilin or profilin-actin, and a characteristic FH2 domain (a.a. 68–464) implicated in binding to actin (**Figure 1A**). However, one noticeable feature of AtFH19 is that FH1 is followed immediately by FH2; in other words, there is no linker between these domains. In addition, there is no additional sequence after FH2 at the C-terminus, which is quite different from other characterized plant formins (Favery et al. 2004; Deeks et al. 2005; Ingouff et al. 2005; Michelot et al. 2005; Yi et al. 2005; Ye et al. 2009). To characterize the effects of AtFH19 on actin dynamics, we generated two recombinant fusion proteins, AtFH19 FH2 and AtFH19 FH1FH2 (**Figure 1A, B**). Sequence comparisons between the FH2 domain of AtFH19 with that of AtFH1 and Bni1p revealed that AtFH19 FH2 shares 43% and 41% similarity with AtFH1 FH2 and Bni1p FH2, respectively,
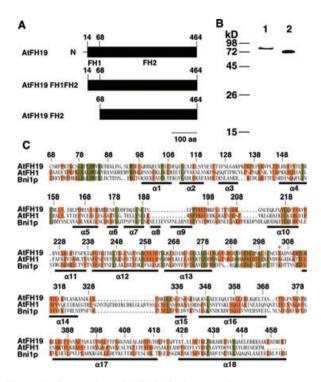
Figure 1. Generation of AtFH19 fusion proteins.

(A) Schematic representation of the predicted domain organization of AtFH19. The FH1 domain comprises amino acids 14–67, and the FH2 domain comprises amino acids 68–464. aa, amino acids.

(B) Coomassie Blue-stained protein gel of purified recombinant formin proteins. Lane 1, GST-AtFH19 FH1FH2 protein; lane 2, GST-AtFH19 FH2 protein. Recombinant GST-AtFH19 FH1FH2–6His and GST-AtFH19 FH2–6His fusion proteins include amino acids 14–464 and 68–464, respectively.

(C) Sequence alignment of the AtFH19 FH2 domain with the equivalent domains from budding yeast Bni1p and AtFH1, based on the structure of the FH2 domain of Bni1p (Xu et al. 2004). Multiple sequence alignment was performed with DNAMAN (6.0.40). Second structures were marked below the sequence based on the information of the Bni1p crystal structure (Protein Data Bank ID 1UX5) done with EsPript (http://espript.ibcp.fr/ESPript/ESPript/). The names and database accession numbers for the sequences are as follows: AtFH1 (*Arabidopsis thaliana* formin1, NP_189177), AtFH19 (BAD94830), and Bni1p (NP_014128). Helices are indicated by bars below the alignment. The asterisk above the alignment marks R305 in AtFH19. The numbers shown above the alignment correspond to the AtFH19 sequence. The residues highlighted with green represent amino acids with 100% identity, and the residues highlighted with orange represent amino acids with identity greater than 50%.

and retains several highly-conserved residues (**Figure 1C**). This implies that AtFH19 may have conserved activities on actin.

AtFH19 nucleates actin assembly

To determine whether AtFH19 nucleates actin assembly, we initially used a pyrene–actin polymerization assay. As shown in **Figure 2A**, AtFH19 FH1FH2 eliminates the nucleation step of actin assembly in a dose-dependent manner. Similar results were obtained for AtFH1 FH1FH2 (data not shown). However, a lower AtFH1 FH1FH2 concentration is required to generate the same amount of filament ends (**Figure 2B**). In contrast, AtFH19 FH2, which is lacking the FH1 domain, has barely detectable nucleation activity (data not shown). Interestingly, AtFH19 FH2 inhibits actin nucleation from actin monomers induced by AtFH19 FH1FH2, suggesting that AtFH19 FH2 competes with AtFH19 FH1FH2 in binding to actin monomers or actin filament ends (**Figure 2C**). We also visualized the effect of AtFH19 on actin assembly by fluorescence microscopy and found that the presence of AtFH19 FH1FH2 and AtFH1 FH1FH2 reduced the mean length ($\pm SE$) of actin filaments from 14.50 ± 1.14 μm ($n = 150$) (**Figure 2G**) to 4.0 ± 0.3 μm ($n = 150$) (**Figure 2H**), and 0.77 ± 0.03 μm ($n = 150$) (**Figure 2I**), respectively. We also found that AtFH19 FH1FH2 could nucleate actin assembly from actin bound to profilin (**Figure 2J**); however, the effect was very weak compared to that of AtFH1 FH1FH2 (Figure S1). Regardless, the ability of AtFH19 FH1FH2 to assemble actin from profilin-actin confirms that polymerization occurs at the barbed end of filaments. To rule out the possibility that the first 13 a.a. are part of the FH1 domain and regulate its nucleation activity, we generated the full-length AtFH19 protein. Our results show that the activity of AtFH19 did not make any major difference to actin assembly from actin monomers and the profilin-actin complex compared to that of AtFH19 FH1FH2 (Figure S2). However, because the yield of purified recombinant full-length AtFH19 was rather low compared to that of AtFH19 FH1FH2, we used AtFH19 FH1FH2 protein in the following studies.

The ability of AtFH19 FH1FH2 to nucleate actin assembly from profilin-actin was also visualized directly and in real-time using total internal reflection fluorescence microscopy (TIRFM). Compared to profilin-actin alone (**Figure 3A–E** and Movie S1), the presence of AtFH19 FH1FH2 increased the number of actin filaments in the field significantly (**Figure 3F–J** and Movie S2). The average number ($\pm SE$) of actin filaments per field increased from 3.0 ± 0.8 ($n = 6$) for profilin–actin alone to 28.1 ± 2.5 ($n = 6$) in the presence of 100 nM AtFH19 FH1FH2 (**Figure 3K**). The TIRFM assay unambiguously supports the notion that AtFH19 does indeed nucleate actin assembly from a pool of actin monomers bound to profilin.

AtFH19 caps actin filament barbed ends

To determine whether AtFH19 caps the barbed end of actin filaments, a seeded actin elongation assay was employed.
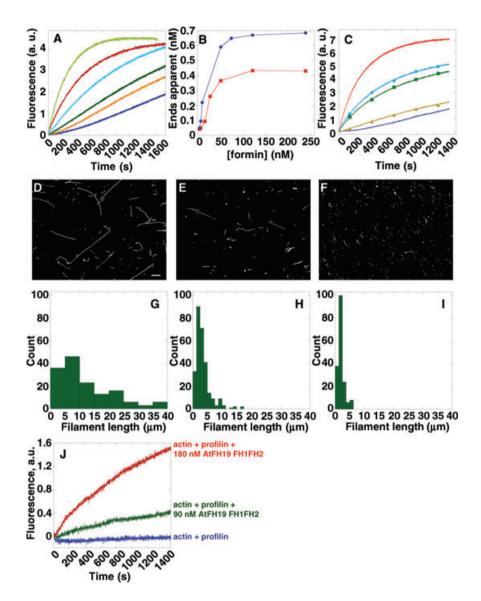
Figure 2. AtFH19 FH1FH2 nucleates actin assembly from actin monomers or actin monomers bound to profilin.

(A) Time course of actin polymerization in the presence of AtFH19 FH1FH2, monitored by pyrene fluorescence. Different concentrations of AtFH19 FH1FH2 were added to 2 μM of 10% pyrene-labeled actin before initiation of actin polymerization. AtFH19 FH1FH2 concentrations from bottom to top are: 0, 1.5, 3, 12, 25, and 120 nM. a.u., arbitrary fluorescence units.

(B) Nucleation efficiency of AtFH19 FH1FH2. The efficiency of nucleation for AtFH1 FH1FH2 (closed circles) and AtFH19 FH1FH2 (closed squares) was determined at half-maximal polymerization according to Blanchoin et al. (2000).

(C) AtFH19 FH2 inhibits actin nucleation from actin monomers induced by AtFH19 FH1FH2. The curves from top to bottom are: 2 μM G-actin + 180 nM AtFH19 FH1FH2 (open squares), 2 μM G-actin + 180 nM AtFH19 FH1FH2 + 100 nM AtFH19 FH2 (closed circles), 2 μM G-actin + 180 nM AtFH19 FH1FH2 + 200 nM AtFH19 FH2 (closed squares), 2 μM G-actin + 180 nM AtFH19 FH1FH2 + 400 nM AtFH19 FH2 (closed triangles), and 2 μM G-actin alone (open circles).

(D–F) Micrograph of actin filaments for actin alone **(D)**, actin + 200 nM AtFH19 FH1FH2 **(E)**, and actin + 200 nM AtFH1 FH1FH2 **(F)**. The bar in **(D)** represents 10 μm.

(G–I) Histogram of actin filament length distribution for actin alone **(G)**, actin + 200 nM AtFH19 FH1FH2 **(H)**, and actin + 200 nM AtFH1 FH1FH2 **(I)**.

(J) Time course of actin polymerization in the presence of equimolar human profilin I monitored by pyrene fluorescence. Curves from bottom to top are: 2 μM G-actin + 2 μM human profilin I, 2 μM G-actin + 2 μM human profilin I + 90 nM AtFH19 FH1FH2, and 2 μM G-actin + 2 μM human profilin I + 180 nM AtFH19 FH1FH2.
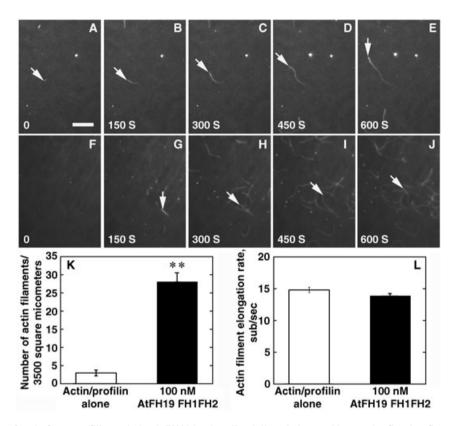
Figure 3. Nucleation of actin from profilin-actin by AtFH19 is visualized directly by total internal reflection fluorescence microscopy (TIRFM).

Time-lapse evanescent wave microscopy was used to monitor nucleation and assembly of actin filaments in the presence or absence of AtFH19 FH1FH2. The white arrows track the end of a representative actin filament during elongation. The time of acquisition for each image is labeled at the bottom of each micrograph. Conditions: 10 mM imidazole, pH 7.0, 50 mM KCl, 1 mM ethyleneglycoltetraacetic, 1 mM $MgCl_2$, 0.2 mM adenosine triphosphate, 50 mM DTT, 50 μM $CaCl_2$, 15 mM glucose, 20 μg/mL catalase, 100 μg/mL glucose oxidase, 1.0% methylcellulose. The bar in **(A)** is 10 μm.

(A–E) Time-lapse series of profilin/Oregon-Green-actin polymerization. We injected 1.5 μM Mg^{2+} adenosine triphosphate (ATP) actin (33.3% Oregon Green-labeled) plus 3 μM human profilin I into a flow cell previously coated with NEM-myosin to facilitate adhesion of actin filaments to the glass cover.

(F–J) Time-lapse series showing the effect of AtFH19 FH1FH2 on actin nucleation. We injected 1.5 μM Mg^{2+} adenosine triphosphate actin (33.3% Oregon Green-labeled) plus 3 μM human profilin I into a flow cell that was coated with NEM-myosin and 100 nM AtFH19 FH1FH2.

(K) Plot of average number of actin filaments per field. The presence of 100 nM AtFH19 FH1FH2 on the cover glass increases the number of actin filaments in the field. Error bars represent mean $\pm$ SE, $n = 6$, **$P < 0.001$.

(L) Plot of average elongation rate of actin filaments.

AtFH19 FH1FH2 inhibited actin polymerization rates in a dose-dependent manner, indicating that it binds to and caps the barbed end of actin filaments (**Figure 4A**). Similar results were obtained with AtFH1 FH1FH2, albeit with lower protein concentrations required to achieve the same effect (**Figure 4B**). In contrast, AtFH19 FH2 did not inhibit elongation, suggesting that it is not capable of capping (data not shown). A mean K_d value ($\pm$SD) of 57.5 $\pm$ 6.9 nM ($n = 3$) for AtFH19 FH1FH2 binding to actin filament barbed ends was calculated. For comparison, a mean K_d value ($\pm$SD) of 36.3 $\pm$ 3.1 nM ($n = 3$)

for AtFH1 FH1FH2 was determined, which is very close to the published value (Michelot et al. 2005). The barbed end capping activity of AtFH19 was further evaluated by applying an actin filament annealing assay. Both AtFH19 FH1FH2 and AtFH1 FH1FH2 slowed actin filament annealing compared to a buffer only control (Figure S3A–C). However, AtFH1 FH1FH2 (Figure S3G–I) inhibited actin filament annealing more strongly than AtFH19 FH1FH2 (Figure S3D–F). This provides further confirmation that AtFH19 FH1FH2 blocks the availability of filament barbed ends.
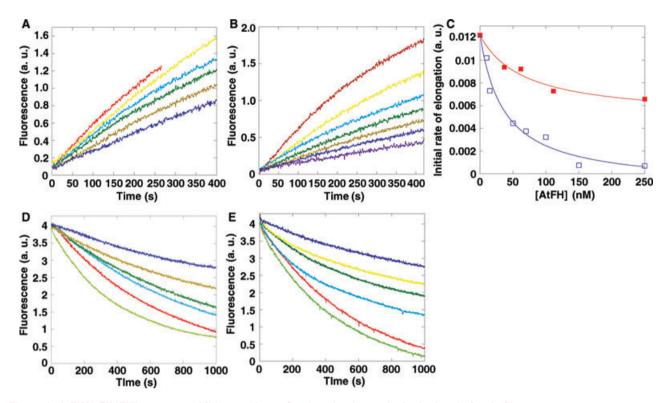
Figure 4. AtFH19 FH1FH2 prevents addition and loss of actin subunits on the barbed end of actin filaments.
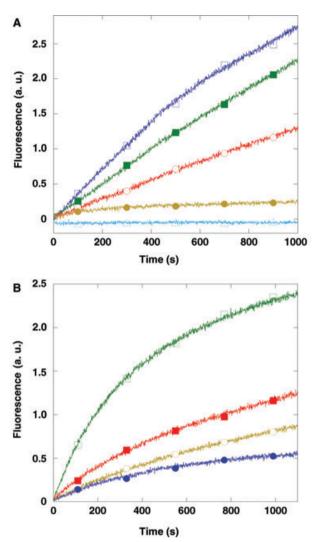
(A–C) AtFH19 FH1FH2 inhibits elongation of actin filaments. **(A)** AtFH19 FH1FH2 concentrations from top to bottom are: 0, 5, 10, 45, 60, and 120 nM. **(B)** AtFH1 FH1FH2 concentrations from top to bottom are: 0, 12, 25, 35, 45, 75, and 250 nM. **(C)** Initial rates of elongation versus AtFH19 FH1FH2 (closed squares) and AtFH1 FH1FH2 (open squares) concentrations were plotted for the representative experiments in **(A)** and **(B)**. The data were fit with Equation 1 (Supporting Information) to determine the dissociation equilibrium constant value of 53 nM for AtFH19 FH1FH2 and 30 nM for AtFH1 FH1FH2. a.u., arbitrary fluorescence units.

(D, E) AtFH19 FH1FH2 inhibits dilution-mediated actin depolymerization. Formin proteins were incubated with 5 μM F-actin for 5 min before being diluted 25 fold. **(D)** Depolymerization of actin filaments in the presence of various concentrations of AtFH19 FH1FH2. AtFH19 FH1FH2 concentrations from bottom to top are: 0, 120, 175, 200, 350, and 450 nM. **(E)** Depolymerization of actin filaments in the presence of various concentrations of AtFH1 FH1FH2. AtFH1 FH1FH2 concentrations from bottom to top are: 0, 90, 140, 180, 280, and 350 nM.

It has been demonstrated for some formins that binding to the barbed end of actin filaments prevents actin depolymerization from the same end (Kovar et al. 2003; Michelot et al. 2005; Yi et al. 2005; Ye et al. 2009). Indeed, AtFH19 FH1FH2 inhibited actin depolymerization in a dose-dependent manner, adding further support for its barbed end capping ability (**Figure 4D**). Similar results were obtained with AtFH1 FH1FH2 (**Figure 4E**). Again, lower concentrations of AtFH1 FH1FH2 were required to achieve the same level of inhibition. To determine whether AtFH19 has bundling activity and contributes to the stabilizing activity in the depolymerization assay, we performed a low-speed co-sedimentation assay and found that AtFH19 FH1FH2 does not bundle actin filaments, in contrast to AtFH1 FH1FH2 (Figure S4) (Michelot et al. 2005). Therefore, we conclude that the inhibitory effect of AtFH19 FH1FH2 on actin depolymerization is due mainly to its barbed end capping activity.

AtFH19 antagonizes the effect of AtFH1 on actin

The expression data from community microarray databases shows that both AtFH1 and AtFH19 are expressed throughout the plant in many of the same tissues (Schmid et al. 2005), although AtFH19 is generally less abundant. The different effects of AtFH1 and AtFH19 on actin dynamics provide an opportunity to determine whether these isoforms function cooperatively or antagonistically to regulate actin assembly. To determine this, actin nucleation and elongation assays were employed. AtFH1 FH1FH2 efficiently nucleates actin assembly from profilin-actin (**Figure 5A**), but AtFH19 FH1FH2 is markedly less efficient, consistent with the results shown previously (Figure S1). Adding AtFH19 FH1FH2 to reactions containing AtFH1 FH1FH2 suppressed nucleation by AtFH1 in a dose-dependent manner. However, these reactions were

Figure 5. AtFH19 FH1FH2 antagonizes the effect of AtFH1 FH1FH2 on actin dynamics.

(A) Actin assembly from profilin-actin in the absence or presence of AtFH19 FH1FH2 and/or AtFH1 FH1FH2. The curves from top to bottom are: 2 µM actin + 2 µM human profilin I + 300 nM AtFH1 FH1FH2 (open squares), 2 µM actin + 2 µM human profilin I + 300 nM AtFH1 FH1FH2 + 250 nM AtFH19 FH1FH2 (closed squares), 2 µM actin + 2 µM human profilin I + 300 nM AtFH1 FH1FH2 + 600 nM AtFH19 FH1FH2 (open circles), 2 µM actin + 2 µM human profilin I + 600 nM AtFH19 FH1FH2 (closed circles), and 2 µM G-actin + 2 µM human profilin I (open triangles). a.u., arbitrary fluorescence units.

(B) AtFH19 FH1FH2 or AtFH1 FH1FH2 partially inhibits actin elongation, but these two compete with each other for actin filament barbed ends. From top to bottom, AtFH proteins in each curve are: no AtFH proteins (open squares), 200 nM AtFH1 FH1FH2 (closed squares), 200 nM AtFH1 FH1FH2 + 450 nM AtFH19 FH1FH2 (open circles), and 450 nM AtFH19 FH1FH2 (closed circles).

still faster compared to AtFH19 FH1FH2 alone at the same concentration, indicating that AtFH19 and AtFH1 may compete for the profilin-actin complex (**Figure 5A**). Alternatively, AtFH19 and AtFH1 may compete for the barbed end of actin filaments. To test this, a seeded actin elongation assay was employed. As shown in **Figure 5B**, incubation of actin filaments seeds with either 200 nM AtFH1 FH1FH2 or 450 nM AtFH19 FH1FH2 inhibited elongation and confirmed the formins' partial barbed end capping activity, consistent with results shown above (**Figure 4A, B**). Incubation of F-actin seeds with both AtFH19 FH1FH2 and AtFH1 FH1FH2 inhibited barbed end elongation, but the effect fell between 200 nM for AtFH1 FH1FH2 alone and 450 nM for AtFH19 FH1FH2 alone (**Figure 5B**). This suggests that AtFH19 FH1FH2 competes with AtFH1 FH1FH2 for the barbed end of actin filaments. Given that both AtFH1 (Michelot et al. 2006) and AtFH19 (**Figure 3F–J** and Movie S2) are non-processive formins, both AtFH19 and AtFH1 may fall off the barbed end of actin filaments after nucleation and leave the barbed end of actin filaments naked. The vacated barbed ends can then subsequently be occupied by either AtFH19 or AtFH1. Given that both formins have similar K_d values for the barbed end (**Figure 4C**), an alternative hypothesis is that AtFH19 and AtFH1 occupy different filament ends and have different elongation rates for the addition of profilin-actin. Based on the primary evidence from the pyrene-actin assembly assay, we predict that the AtFH19 FH1FH2 capped actin filaments elongate slower than AtFH1 FH1FH2-associated actin filaments.

To test this hypothesis, we performed a modified TIRFM assay to visualize actin elongation from nucleation sites on cover glass coated with AtFH1 FH1FH2. Actin elongation could then be tested in the presence of profilin-actin alone, or with additional soluble AtFH1 or AtFH19. We observed that it was easy to monitor numerous elongating actin filaments, presumably nucleated by AtFH1 FH1FH2 attached to the cover glass. Several actin filaments grew out from the same location, as shown in **Figure 6A–E** (see also Movie S3) and reported previously (Michelot et al. 2006). Considering that AtFH1 FH1FH2 is a non-processive formin (Michelot et al. 2006), we assumed that the end of the filament distal to the site of origination represents the barbed end. When 1.5 µM of profilin–actin complex alone was injected into the perfusion chamber, the elongation rate of individual actin filaments was determined to be 9.98 ± 0.32 subunits/s ($n = 10$), which was very close to previously published values (Michelot et al. 2005; Ye et al. 2009). When 10 nM AtFH1 FH1FH2 was co-injected with 1.5 µM profilin-actin into the perfusion chamber with AtFH1 pre-attached to cover glass, the elongation rate was determined to be 10.49 ± 0.26 subunits/s ($n = 12$) (**Figure 6F–J** and Movie S4), which was not significantly different from profilin-actin alone. By comparison, when 10 nM AtFH19 FH1FH2 was co-injected with 1.5 µM profilin-actin into the perfusion chamber with AtFH1
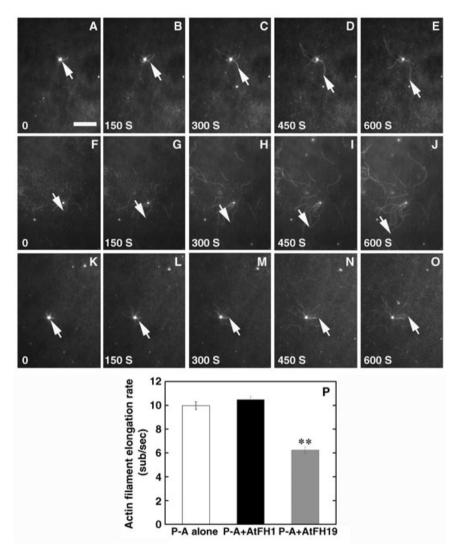
Figure 6. AtFH19 slows down the elongation rate of actin filaments generated by AtFH1.

Time-lapse evanescent wave microscopy of actin filaments nucleated from AtFH1-coated cover glass, in the presence and absence of AtFH19 in solution. White arrows show elongation of representative actin filaments. Elapsed time is recorded at the bottom of each image. Conditions are the same as described in **Figure 3**, except all flow chambers were pre-treated with NEM-myosin and 50 nM AtFH1 FH1FH2. The bar in **(A)** is 10 μm.

(A–E) Time-lapse micrographs of actin filaments generated by AtFH1 FH1FH2 on the cover glass. We injected 1.5 μM Mg^{2+} adenosine triphosphate (ATP) actin (33.3% Oregon Green-labeled) plus 3 μM human profilin I into the flow cell and monitored polymerization by total internal reflection fluorescence microscopy (TIRFM).

(F–J) Time-lapse micrographs of the effect of soluble AtFH1 FH1FH2 on the elongation rate of actin filaments nucleated by AtFH1 FH1FH2. We injected 1.5 μM Mg^{2+}-ATP-actin (33.3% Oregon Green-labeled) plus 3 μM human profilin I and 10 nM AtFH1 FH1FH2 into a flow cell and monitored filament elongation by TIRFM.

(K–O) Time-lapse micrographs of the effect of soluble AtFH19 FH1FH2 on the elongation rate of actin filaments nucleated by AtFH1 FH1FH2. We injected 1.5 μM Mg^{2+}-ATP-actin (33.3% Oregon Green-labeled) plus 3 μM human profilin I and 10 nM AtFH19 FH1FH2 into a flow cell and monitored filament elongation by TIRFM.

(P) Plot of the elongation rate of actin filaments nucleated by AtFH1 FH1FH2 in the presence and absence of AtFH19. White column, black column, and gray column represent elongation rate of actin filaments for actin alone, actin + 10 nM AtFH1 FH1FH2, and actin + 10 nM AtFH19 FH1FH2, respectively. Values represent mean ± SE, $n > 10$. The elongation rate of actin filaments in the presence of AtFH19 FH1FH2 is significantly slower than that in the presence of AtFH1 FH1FH2 (Student's *t*-test, **$P < 0.001$).

pre-attached to cover glass, the elongation rate was determined to be 6.25 ± 0.26 subunits/s ($n = 17$) (**Figure 6K–O** and Movie S5), which indicates that AtFH19 FH1FH2 binds to the barbed end of actin filaments and slows down the elongation rate significantly ($P < 0.001$). Considering the situation that both AtFH1 FH1FH2 and AtFH19 FH1FH2 bind to the barbed end of actin filaments with roughly the same affinity (**Figure 4C**), our interpretation is that AtFH19 FH1FH2-capped actin filaments elongate slower than AtFH1 FH1FH2-capped actin filaments. Therefore, the results from the bulk pyrene-actin assay (**Figure 5B**) could be interpreted as the following: AtFH1 FH1FH2 and AtFH19 FH1FH2 compete with each other to bind to the barbed end of actin filaments, but AtFH19 FH1FH2-capped actin filaments elongate slower than AtFH1 FH1FH2-capped actin filaments.

Discussion

AtFH19 retains the general activities of a formin family member

AtFH19 is a class II formin; it does not contain the characteristic transmembrane domain of class I formins (Blanchoin and Staiger 2010). However, it has a typical polyproline-stretch FH1 domain and a typical FH2 domain (**Figure 1A**). The presence of two characteristic formin-homology domains implies that AtFH19 may retain all the general activities of formins. Indeed, AtFH19 was shown to nucleate actin assembly in the presence or absence of profilin (**Figure 2**), and cap the barbed end of actin filaments (**Figure 4**). However, the AtFH19 construct which comprises only the FH2 domain has only barely detectable nucleation activity (data not shown). Lack of nucleation activity by the construct AtFH19 FH2 alone suggests that the presence of FH1 is required for AtFH19-mediated formation of actin nuclei. The presence of an FH1 domain may contribute to the dimer formation of FH2, which was shown to be necessary for the nucleation activity of Bni1p (Xu et al. 2004). Interestingly, AtFH19 FH2 inhibits actin nucleation induced by AtFH19 FH1FH2 (**Figure 2C**), suggesting that AtFH19 FH2 may compete directly with AtFH19 FH1FH2 for binding actin monomers. AtFH19 FH1FH2 caps barbed ends, but still allows elongation to occur in the presence of AtFH19 (**Figure 4A**), which is similar to FH1FH2 of AtFH1, AtFH3, and AtFH5 (Ingouff et al. 2005; Michelot et al. 2005; Ye et al. 2009), but different from FH1FH2 of Cdc12 from fission yeast (*Schizosaccharomyces pombe*), which requires profilin to bind to the FH1 domain and allow the addition of actin monomers onto the barbed end (Kovar et al. 2003). This behavior of AtFH19 FH1FH2 on actin elongation is in agreement with the "leaky capping" property previously reported for Bni1p (Zigmond et al. 2003). However, direct visualization of AtFH19-induced actin assembly from profilin-actin by TIRFM indicates that AtFH19

is most likely a non-processive formin (**Figure 3F–J** and Movie S2). We also tested whether AtFH19 has extra biochemical activities, such as bundling activity which has been shown in AtFH1, FRLα, mDia2, and Bnr1p (Michelot et al. 2005; Moseley and Goode 2005; Harris et al. 2006) or severing activity shown in FRLα and AtFH8 (Harris et al. 2004; Yi et al. 2005). However, AtFH19 lacks bundling activity (Figure S4) and severing activity (**Figure 3F–J**). In summary, AtFH19 retains the general activities of a formin including nucleating actin assembly from actin monomers and actin monomers bound to profilin, and capping the barbed end of actin filaments to prevent the addition and loss of actin subunits at the same end.

AtFH19 has quantitatively different effects on actin compared to AtFH1

We characterized AtFH19 and found that it has biochemical activities that distinguish it from the well-characterized class I formin AtFH1. To figure out the potential reason for the difference of the activities between AtFH19 and AtFH1, we aligned the AtFH19 FH2 sequence to that of AtFH1 and Bni1p to look for the residues that could explain these differences. A noticeable difference is that a conserved lysine which lies on the interaction surface with actin (Xu et al. 2004) has been replaced with arginine at position 305 in AtFH19 (**Figure 1C**). However, substitution with a similarly charged a.a. may not affect the interaction between actin and formin. We also performed homology modeling for AtFH19 FH2 and AtFH1 FH2 using the structure of the Bni1p FH2 domain. We found that AtFH19 has a smaller surface contact area at the lasso/post interface than does AtFH1, and a lower electrostatic surface potential in a small region around R305 compared to AtFH1 around K825 (Figure S5C–E). This may affect the formation and stability of the FH2 dimer, consequently affecting its activity on actin. However, this needs to be demonstrated by point mutations and deletion analysis in the future.

In addition, compared to AtFH1 and other characterized formins (Ingouff et al. 2005; Michelot et al. 2005; Yi et al. 2005; Ye et al. 2009), the FH2 domain follows the FH1 domain immediately in AtFH19 (**Figure 1A**). This may affect the ability of AtFH19 to use the profilin-actin complex and may alter the elongation rate of AtFH19-capped actin filaments. Although the exact mechanism by which formin facilitates the addition of the profilin-actin complex onto the barbed end is not well understood, it is proposed that FH1 binds to the profilin-actin complex and increases the local concentration of actin, subsequently delivering actin to the FH2-bound actin barbed end (Romero et al. 2004; Kovar et al. 2006; Vavylonis et al. 2006; Paul and Pollard 2008). The lack of a linker between FH1 and FH2 in AtFH19 may affect the flexibility of this molecule, consequently affecting the transfer of actin to FH2-bound filament barbed ends, and partially accounting for the low efficiency of AtFH19

in nucleating actin assembly from profilin-actin (**Figure 2H**). This hypothesis could be tested by adding a linker between FH1 and FH2 of AtFH19. These activity differences between the two formin isoforms AtFH1 and AtFH19 could be tailored to different requirements for actin assembly in the plant cell.
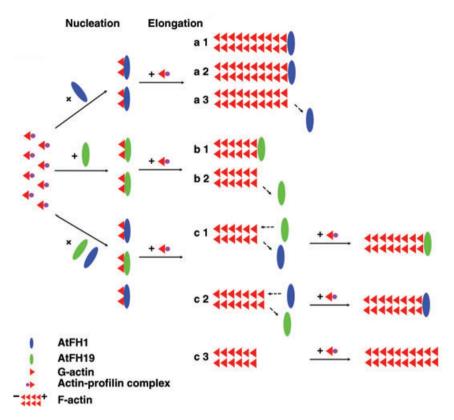
A general mechanism for plant formin isoform competition and its effects on actin dynamics

The number of formin genes isolated from plants has expanded significantly (Cvrckova et al. 2004; Blanchoin and Staiger 2010). How these isoforms coordinate to regulate actin dynamics remains a mystery. Here, we showed that a class II formin, AtFH19, has quantitatively different effects on actin dynamics compared to another well-characterized class I formin, AtFH1 (Cheung and Wu 2004; Michelot et al. 2005; Michelot et al. 2006). This provides a good opportunity to determine how these two formins might coordinate to regulate actin dynamics. Based on the *in vitro* biochemical data, we proposed a simple model of the coordination of AtFH19 with AtFH1 in regulating actin dynamics (**Figure 7**). Our model is that both AtFH19 and AtFH1 can nucleate actin assembly from profilin-actin, but AtFH1 is more efficient than AtFH19. In the presence of AtFH1 alone, AtFH1 nucleates actin assembly and falls off the barbed end of actin filaments, and the nucleated actin filaments are subsequently elongated by profilin-actin (**Figure 7a1–a3**) (Michelot et al. 2006). According to our TIRFM data (**Figure 3F–J** and Movie S2), AtFH19 is very likely a non-processive formin as well. Therefore, in the presence of AtFH19 alone, actin filaments are nucleated by AtFH19, and, like AtFH1, AtFH19 will also fall off the barbed end of actin filaments after it is nucleated. AtFH19-capped actin filaments are predicted to elongate slowly (**Figure 7b1**) as suggested by the TIRFM data (**Figure 6**). In the presence of both AtFH1 and AtFH19, they may compete to bind to profilin–actin complexes during the nucleation phase, and barbed ends during subsequent filament elongation. The final nucleation efficiency is determined by the molar ratio between AtFH19 and AtFH1. Considering the non-processive property of both AtFH1 (Michelot et al. 2006) and AtFH19 (see Movie S2), actin filaments nucleated by AtFH1 or AtFH19 could either be elongated by profilin–actin after they fall off the barbed end of actin filaments (**Figure 7c3**), or the vacated barbed ends could be subsequently occupied by AtFH19 or AtFH1 (**Figure 7c1, c2**). However, the bulk pyrene–actin assay (**Figure 5**) and TIRFM assay (**Figure 6**) indicate that AtFH19-capped actin filaments elongate slower than AtFH1-capped actin filaments. Therefore, the actin polymerization level and individual elongation rates may be determined by the total concentration and molar ratio of these formins. The coordination between AtFH1 and AtFH19 may be biologically-relevant, and could extend to the coordination of other quantitatively different formins in the plant cell.

Materials and Methods

Protein purification

To express fusion proteins for AtFH19 FH1-FH2 and AtFH19 FH2, the coding sequences for these two constructs were amplified by polymerase chain reaction (PCR) from a RAFL clone (pda15411 containing AtFH19 cDNA; RIKEN BioResource Center, Japan). The forward primers used for amplifying AtFH19 FH1FH2 and AtFH19 FH2 were 5′-GT<u>GGATCC</u>AACCTCTTCCACCACCACCTCCT-3′ (with the BamH I site underlined) and 5′-GT<u>GGATCC</u>TGTTCACGTCCACCTAAAA-3′ (with the BamH I site underlined), respectively. The reverse primers used for amplifying AtFH19 FH1FH2 and AtFH19 FH2 were 5′-CC<u>CTCGAG</u>ATGGTGATGGTGATGGTGCTTCGTCTTCTCCATTT-3′ (with the Xho I site underlined) and 5′-CC<u>CTCGAG</u>TTACTTCGTCTT CTCCATTT-3′ (with the Xho I site underlined), respectively. Amplified sequences were A-tailed and cloned into the pMD19-T vector at corresponding sites designed in the primers (TaKaRa Biotechnology, Dalian, China). The cDNA sequences were verified by sequencing. GST-AtFH19 FH1FH2 and GST-AtFH19 FH2 fusion proteins were expressed in the Rosetta (DE3) strain of *Escherichia coli* (Invitrogen) by induction with 0.4 mM isopropyl β-D-thiogalactopyranoside overnight at 16 °C. Cultures were collected by centrifugation at 4 307 *g* and were resuspended in phosphate-buffered saline (140 mM NaCl, 2.7 mM KCl, 10 mM Na_2HPO_4, 1.8 mM KH_2PO_4, pH 7.4) containing a proteinase inhibitor cocktail (Ren et al. 1997). After sonication, extracts were clarified by centrifugation at 45 000 g. The GST-fusion proteins were initially purified by chromatography on a glutathione-Sepharose column and eluted with 10 mM glutathione in 50 mM Tris/HCl, pH 8.5. After dialysis against the binding buffer (25 mM Tris/HCl, pH 7.9, 250 mM KCl, 5 mM imidazole, 2 mM β-mercaptoethanol), the fusion proteins were incubated with a Ni-NTA resin (Novagen). After being washed with washing buffer (25 mM Tris/HCl, pH 7.9, 250 mM KCl, 20 mM imidazole, 2 mM β-mercaptoethanethanol), the fusion proteins were eluted with elution buffer (25 mM Tris/HCl, pH 7.9, 250 mM KCl, 600 mM imidazole, 2 mM β-mercaptoethanethiol). The fusion proteins were dialyzed against 1 × KMEI (10 mM imidazole, pH 7.0, 100 mM KCl, 1 mM ethyleneglycoltetraacetic (EGTA), 1 mM $MgCl_2$). GST-AtFH19 FH1FH2 was used immediately after purification without freezing. GST-AtFH19 FH2 was flash frozen in liquid nitrogen and stored at −80 °C. The protein concentration was determined by Bradford assay using bovine serum albumin (BSA) as the standard. Muscle actin was purified from skeletal muscle acetone powder of rabbit according to Spudich and Watt (1971), and monomeric Ca adenosine triphosphate (ATP) actin was further purified by Sephacryl S-300 chromatography at 4 °C in G buffer (5 mM Tris/HCl, pH 8, 0.2 mM ATP, 0.1 mM $CaCl_2$, 0.5 mM DL-dithiothreitol

Figure 7. A simple model for the coordination of AtFH19 with AtFH1 on actin assembly.

Based on the *in vitro* biochemical data, both AtFH19 and AtFH1 can nucleate actin assembly from profilin–actin, although AtFH1 is more efficient. Considering the fact that AtFH1 is a non-processive formin (Michelot et al. 2006) and AtFH19 is very likely also a non-processive formin (Movie S2), actin filaments formed in the presence of either AtFH1 alone or AtFH19 alone could either be capped or naked (a1, a2, a3, b1, and b2), but actin filaments capped with AtFH19 elongate slowly (a1, a2, a3, b1, and b2). In the presence of both AtFH1 and AtFH19, AtFH1 and AtFH19 will compete to bind the profilin–actin complex at the nucleation phase, and the formed actin filaments could be AtFH1-capped actin filaments, AtFH19-capped actin filaments, or naked actin filaments in the population (c1, c2, and c3). The situation is totally dependent on the total concentration and molar ratio of these formins. The final actin polymerization level could be determined by the molar ratio of these two formins for efficient nucleation and apparent elongation rate.

(DTT), 0.1 mM azide) (Pollard 1984). For monitoring the kinetic process of actin polymerization, actin was labeled on Cys-374 with pyrene iodoacetamide (Pollard 1984). Human profilin I, AtFH1 FH1FH2, and AtFH1 FH2 were purified according to previously reported methods (Fedorov et al. 1994; Michelot et al. 2005).

Low speed co-sedimentation assay, actin nucleation assay, elongation assay, actin depolymerization assay, and fluorescence microscopy of actin filaments

These experimental procedures were carried out according to previously published methods (Higgs et al. 1999; Blanchoin et al. 2000; Huang et al. 2003; Huang et al. 2005; Michelot et al.

2005). For a detailed protocol, see the supporting information online (Supporting Information).

Visualization of actin assembly by TIRFM

To analyze actin filament polymerization of single filaments in real-time, we conducted TIRFM experiments according to established methods (Kovar and Pollard 2004). The flow cell was incubated with 100 nM N-ethylmaleimide myosin for 2 min, followed by incubation with AtFH1 FH1FH2 or AtFH19 FH1FH2. The flow cell was then equilibrated with 1% BSA, and finally washed with $1 \times$ TIRFM buffer (10 mM imidazole, pH 7.0, 50 mM KCl, 1 mM $MgCl_2$, 1 mM EGTA, 50 mM DTT, 0.2 mM ATP, 50 μM $CaCl_2$, 15 mM glucose, 20 μg/mL

catalase, 100 µg/mL glucose oxidase, 1.0% methylcellulose). Subsequently, 1.5 µM Mg^{2+}-ATP-actin (33.3% Oregon Green-labeled) was injected into the flow cell. We started to acquire the time lapse of images as soon as the focal plane was found. To determine the effect of AtFH19 FH1FH2 on the elongation of actin filaments generated by AtFH1 FH1FH2, 10 nM AtFH19 FH1FH2 was co-injected with 1.5 µM Mg^{2+}-ATP-actin (33.3% Oregon Green-labeled) into the flow cell. We observed the actin filaments by TIRFM illumination with a DMI6000CS microscope (Leica, Wetzlar, Germany) equipped with a 100 × 1.46 numerical aperture HC PLANs objective. The digital images were taken with a Photometrics cascade II 512 CCD camera (Major Instruments) using LAS AF software. The interval time was 15 s between two neighboring pictures. The length of actin filaments was measured using Image J software (http://rsbweb.nih.gov/ij/, ver. 1.38).

Acknowledgements

References

Basu D, Le J, El-Essal Sel D, Huang S, Zhang C, Mallery EL, Koliantz G, Staiger CJ, Szymanski DB (2005) DISTORTED3/SCAR2 is a putative *Arabidopsis* WAVE complex subunit that activates the Arp2/3 complex and is required for epidermal morphogenesis. *Plant Cell* **17,** 502–524.

Blanchoin L, Staiger CJ (2010) Plant formins: Diverse isoforms and unique molecular mechanism. *Biochim. Biophys. Acta* **1803,** 201–206.

Blanchoin L, Amann KJ, Higgs HN, Marchand JB, Kaiser DA, Pollard TD (2000) Direct observation of dendritic actin filament networks nucleated by Arp2/3 complex and WASP/Scar proteins. *Nature* **404,** 1007–1011.

Carlier MF (2011) A new twist in actin filament nucleation. *Nat. Struct. Mol. Biol.* **18,** 967–969.

Chesarone MA, DuPage AG, Goode BL (2010) Unleashing formins to remodel the actin and microtubule cytoskeletons. *Nat. Rev. Mol. Cell Biol.* **11,** 62–74.

Cheung AY, Wu HM (2004) Overexpression of an *Arabidopsis* formin stimulates supernumerary actin cable formation from pollen tube cell membrane. *Plant Cell* **16,** 257–269.

Cvrckova F (2000) Are plant formins integral membrane proteins? *Genome Biol.* **1,** RESEARCH001.

Cvrckova F, Novotny M, Pickova D, Zarsky V (2004) Formin homology 2 domains occur in multiple contexts in angiosperms. *BMC Genomics* **5,** 44.

Deeks MJ, Hussey PJ, Davies B (2002) Formins: Intermediates in signal-transduction cascades that affect cytoskeletal reorganization. *Trends Plant Sci.* **7,** 492–498.

Deeks MJ, Cvrckova F, Machesky LM, Mikitova V, Ketelaar T, Zarsky V, Davies B, Hussey PJ (2005) *Arabidopsis* group Ie formins localize to specific cell membrane domains, interact with actin-binding proteins and cause defects in cell expansion upon aberrant expression. *New Phytol.* **168,** 529–540.

Favery B, Chelysheva LA, Lebris M, Jammes F, Marmagne A, De Almeida-Engler J, Lecomte P, Vaury C, Arkowitz RA, Abad P (2004) *Arabidopsis* formin AtFH6 is a plasma membrane-associated protein upregulated in giant cells induced by parasitic nematodes. *Plant Cell* **16,** 2529–2540.

Fedorov AA, Pollard TD, Almo SC (1994) Purification, characterization and crystallization of human platelet profilin expressed in *Escherichia coli*. *J. Mol. Biol.* **241,** 480–482.

Firat-Karalar EN, Welch MD (2011) New mechanisms and functions of actin nucleation. *Curr. Opin. Cell Biol.* **23,** 4–13.

Grunt M, Zarsky V, Cvrckova F (2008) Roots of angiosperm formins: The evolutionary history of plant FH2 domain-containing proteins. *BMC Evol. Biol.* **8,** 115.

Harris ES, Li F, Higgs HN (2004) The mouse formin, FRLalpha, slows actin filament barbed end elongation, competes with capping protein, accelerates polymerization from monomers, and severs filaments. *J. Biol. Chem.* **279,** 20076–20087.

Harris ES, Rouiller I, Hanein D, Higgs HN (2006) Mechanistic differences in actin bundling activity of two mammalian formins, FRL1 and mDia2. *J. Biol. Chem.* **281,** 14383–14392.

Higashida C, Miyoshi T, Fujita A, Oceguera-Yanez F, Monypenny J, Andou Y, Narumiya S, Watanabe N (2004) Actin polymerization-driven molecular movement of mDia1 in living cells. *Science* **303,** 2007–2010.

Higgs HN (2005) Formin proteins: A domain-based approach. *Trends Biochem. Sci.* **30,** 342–353.

Higgs HN, Peterson KJ (2005) Phylogenetic analysis of the formin homology 2 domain. *Mol. Biol. Cell* **16,** 1–13.

Higgs HN, Blanchoin L, Pollard TD (1999) Influence of the C terminus of Wiskott-Aldrich syndrome protein (WASp) and the Arp2/3 complex on actin polymerization. *Biochemistry* **38,** 15212–15222.

Huang S, Blanchoin L, Kovar DR, Staiger CJ (2003) *Arabidopsis* capping protein (AtCP) is a heterodimer that regulates assembly at the barbed ends of actin filaments. *J. Biol. Chem.* **278,** 44832–44842.

Huang S, Robinson RC, Gao LY, Matsumoto T, Brunet A, Blanchoin L, Staiger CJ (2005) *Arabidopsis* VILLIN1 generates actin filament cables that are resistant to depolymerization. *Plant Cell* **17,** 486–501.

Ingouff M, Fitz Gerald JN, Guerin C, Robert H, Sorensen MB, Van Damme D, Geelen D, Blanchoin L, Berger F (2005) Plant formin AtFH5 is an evolutionarily conserved actin nucleator involved in cytokinesis. *Nat. Cell Biol.* **7,** 374–380.

Kleinebrecht J, Selow J, Winkler W (1982) The mouse mutant limb-deformity (ld). *Anat. Anz.* **152,** 313–324.

Kovar DR, Pollard TD (2004) Insertional assembly of actin filament barbed ends in association with formins produces piconewton forces. *Proc. Natl. Acad. Sci. USA* **101,** 14725–14730.

Kovar D.R, Kuhn JR, Tichy AL, Pollard TD (2003) The fission yeast cytokinesis formin Cdc12p is a barbed end actin filament capping protein gated by profilin. *J. Cell Biol.* **161,** 875–887.

Kovar DR, Harris ES, Mahaffy R, Higgs HN, Pollard TD (2006) Control of the assembly of ATP- and ADP-actin by formins and profilin. *Cell* **124,** 423–435.

Le J, El-Assal Sel D, Basu D, Saad ME, Szymanski DB (2003) Requirements for *Arabidopsis* ATARP2 and ATARP3 during epidermal development. *Curr. Biol.* **13,** 1341–1347.

Li F, Higgs HN (2003) The mouse Formin mDia1 is a potent actin nucleation factor regulated by autoinhibition. *Curr. Biol.* **13,** 1335–1340.

Li S, Blanchoin L, Yang Z, Lord EM (2003) The putative *Arabidopsis* arp2/3 complex controls leaf cell morphogenesis. *Plant Physiol.* **132,** 2034–2044.

Michelot A, Guerin C, Huang S, Ingouff M, Richard S, Rodiuc N, Staiger CJ, Blanchoin L (2005) The formin homology 1 domain modulates the actin nucleation and bundling activity of *Arabidopsis* FORMIN1. *Plant Cell* **17,** 2296–2313.

Michelot A, Derivery E, Paterski-Boujemaa R, Guerin C, Huang S, Parcy F, Staiger CJ, Blanchoin L (2006) A novel mechanism for the formation of actin-filament bundles by a nonprocessive formin. *Curr. Biol.* **16,** 1924–1930.

Moseley JB, Goode BL (2005) Differential activities and regulation of Saccharomyces cerevisiae formin proteins Bni1 and Bnr1 by Bud6. *J. Biol. Chem.* **280,** 28023–28033.

Mullins RD, Heuser JA, Pollard TD (1998) The interaction of Arp2/3 complex with actin: Nucleation, high affinity pointed end capping, and formation of branching networks of filaments. *Proc. Natl. Acad. Sci. USA* **95,** 6181–6186.

Paul AS, Pollard TD (2008) The role of the FH1 domain and profilin in formin-mediated actin-filament elongation and nucleation. *Curr. Biol.* **18,** 9–19.

Pollard TD (1984) Polymerization of ADP-actin. *J. Cell Biol.* **99,** 769–777.

Pollard TD, Borisy GG (2003) Cellular motility driven by assembly and disassembly of actin filaments. *Cell* **112,** 453–465.

Pollard TD, Cooper JA (2009) Actin, a central player in cell shape and movement. *Science* **326,** 1208–1212.

Pruyne D, Evangelista M, Yang C, Bi E, Zigmond S, Bretscher A, Boone C (2002) Role of formins in actin assembly: Nucleation and barbed-end association. *Science* **297,** 612–615.

Ren H, Gibbon BC, Ashworth SL, Sherman DM, Yuan M, Staiger CJ (1997) Actin purified from maize pollen functions in living plant cells. *Plant Cell* **9,** 1445–1457.

Romero S, Le Clainche C, Didry D, Egile C, Pantaloni D, Carlier MF (2004) Formin is a processive motor that requires profilin to accelerate actin assembly and associated ATP hydrolysis. *Cell* **119,** 419–429.

Sagot I, Klee SK, Pellman D (2002a) Yeast formins regulate cell polarity by controlling the assembly of actin cables. *Nat. Cell Biol.* **4,** 42–50.

Sagot I, Rodal AA, Moseley J, Goode BL, Pellman D (2002b) An actin nucleation mechanism mediated by Bni1 and profilin. *Nat. Cell Biol.* **4,** 626–631.

Schmid M, Davison TS, Henz SR, Pape UJ, Demar M, Vingron M, Scholkopf B, Weigel D, Lohmann JU (2005) A gene expression map of *Arabidopsis thaliana* development. *Nat. Genet.* **37,** 501–506.

Spudich JA, Watt S (1971) The regulation of rabbit skeletal muscle contraction. I. Biochemical studies of the interaction of the tropomyosin-troponin complex with actin and the proteolytic fragments of myosin. *J. Biol. Chem.* **246,** 4866–4871.

Vavylonis D, Kovar DR, O'Shaughnessy B, Pollard TD (2006) Model of formin-associated actin filament elongation. *Mol. Cell* **21,** 455–466.

Vidali L, van Gisbergen PA, Guerin C, Franco P, Li M, Burkart GM, Augustine RC, Blanchoin L, Bezanilla M (2009) Rapid formin-mediated actin-filament elongation is essential for polarized plant cell growth. *Proc. Natl. Acad. Sci. USA* **106,** 13341–13346.

Wasteneys GO, Yang Z (2004) New views on the plant cytoskeleton. *Plant Physiol.* **136,** 3884–3891.

Xu Y, Moseley JB, Sagot I, Poy F, Pellman D, Goode BL, Eck MJ (2004) Crystal structures of a formin homology-2 domain reveal a tethered dimer architecture. *Cell* **116,** 711–723.

Yang W, Ren S, Zhang X, Gao M, Ye S, Qi Y, Zheng Y, Wang J, Zeng L, Li Q, Huang S, He Z (2011) BENT UPPERMOST INTERNODE1 encodes the class II formin FH5 crucial for actin organization and rice development. *Plant Cell* **23,** 661–680.

Ye J, Zheng Y, Yan A, Chen N, Wang Z, Huang S, Yang Z (2009) *Arabidopsis* formin3 directs the formation of actin cables and polarized growth in pollen tubes. *Plant Cell* **21,** 3868–3884.

Yi K, Guo C, Chen D, Zhao B, Yang B, Ren H (2005) Cloning and functional characterization of a formin-like protein (AtFH8) from *Arabidopsis*. *Plant Physiol.* **138,** 1071–1082.

Zhang Z, Zhang Y, Tan H, Wang Y, Li G, Liang W, Yuan Z, Hu J, Ren H, Zhang D (2011) RICE MORPHOLOGY DETERMINANT

encodes the type II formin FH5 and regulates rice morphogenesis. *Plant Cell* **23,** 681–700.

Zigmond SH, Evangelista M, Boone C, Yang C, Dar AC, Sicheri F, Forkey J, Pring M (2003) Formin leaky cap allows elongation in the presence of tight capping proteins. *Curr. Biol.* **13,** 1820–1823.

(Co-Editor: Ming Yuan)

Supporting Information

Additional Supporting Information may be found in the online version of this article:

Movie S1. The displaying movie corresponds to the time-lapse series shown in Figure 3A–E.
Movie S2. The displaying movie corresponds to the time-lapse series shown in Figure 3F–J.
Movie S3. The displaying movie corresponds to the time-lapse series shown in Figure 6A–E.
Movie S4. The displaying movie corresponds to the time-lapse series shown in Figure 6F–J.

Movie S5. The displaying movie corresponds to the time-lapse series shown in Figure 6K–O.
Figure S1. AtFH19 FH1FH2 is less efficient than AtFH1 FH1FH2 to nucleate actin assembly from actin bound to profilin.
Figure S2. Full-length AFH19 has similar activity compared to that of AFH19 FH1FH2.
Figure S3. AtFH19 FH1FH2 inhibits end-to-end annealing of actin filaments.
Figure S4. AtFH19 FH1FH2 does not bundle actin filaments.
Figure S5. Homology modeling predicts that the overall fold is virtually identical for the FH2 domain of AtFH19 and AtFH1, but AtFH19 FH2 has lower electrostatic surface potential and lower surface contact area of the lasso/post interface.

Please note: Wiley-Blackwell are not responsible for the content or functionality of any supporting materials supplied by the authors. Any queries (other than missing material) should be directed to the corresponding author for the article.